

# FIXED SINKAGE AND TRIM BARE HULL 5415 SIMULATIONS USING CFDShip-IOWA

Shanti Bhushan, Thad Michael, Jianming Yang, Pablo Carrica, and Frederick Stern  
IHR-Hydroscience and Engineering, The University of Iowa, Iowa City, IA 52242-1585

## 1. SUMMARY

Simulations are performed using CFDShip-Iowa toolbox curvilinear (V4) and Cartesian (V6) grid solvers for straight ahead bare hull 5415 at Reynolds number  $Re = 5.13 \times 10^6$  and Froude number ( $Fr$ ) = 0.28 corresponding to the flow conditions for Case 3.1b in this workshop. The boundary layer and wake profiles are also compared with the higher  $Re$  experimental data for Case 3.1a. V4 simulations include DES on a 300M grid and URANS on a 615K grid. V6 simulations are performed using wall-function wall-layer model on grids up to 276M points. The large grid V4-DES simulation provides significantly better resistance and wave elevation predictions than the coarse grid URANS simulations. V4-DES provides a plausible description of the vortical structures and mean flow patterns observed in the sparse experimental data. However, the vortex strengths are over predicted and the turbulence is not resolved which suggests the need for advance turbulence model. V6 provides good predictions for the wave elevation pattern, but predicts diffused vortical structures due to poor wall-layer predictions. An approximate domain method for the immersed boundary is investigated to address the limitations of the wall-function implementation.

## 2. INTRODUCTION

Bare hull 5415 in straight ahead condition at fixed sinkage and trim for  $Fr = 0.28$  is a well documented validation case for ship hydrodynamics. This case has been previously used at the CFD Workshops Gothenburg 2000 (Larsson et al., 2000) and Tokyo 2005 (Hino, 2005) to assess the state of the art in viscous ship flow computations. The available experimental datasets for this test case include resistance, wave elevation and boundary layer and wake profiles at several axial cross planes at  $Re = 1.2 \times 10^7$  (Olivieri et al., 2001) which are used for case 3.1a in this workshop, and resistance, wave elevation, velocity and turbulence profiles at the nominal wake plane  $x/L = 0.935$  at  $Re = 5.13 \times 10^6$  (Longo et al., 2007) which are used for case 3.1b.

Previously, Wilson and Stern (2002) performed simulations at  $Re = 5.13 \times 10^6$  using CFDShip-Iowa V3, which uses surface-tracking method for free-surface modeling. The study focused on the verification and validation using grids up to 1.78 million (M) points. The averaged comparison error ( $E = D-S$ ) between the experimental data ( $D$ ) and the solution ( $S$ ) was  $4.2\%D$  for the resistance and was validated at  $U_V = 8\%D$  interval, where  $U_V = \sqrt{(U_G^2 + U_D^2)}$ ,  $U_G$  and  $U_D$  are validation, grid and experimental uncertainties,

respectively. The wave elevation and the boundary layer profiles at the nominal wake plane were validated at  $U_V = 6.4\%D$  and  $5.7\%D$  intervals, respectively. Recently, Sakamoto et al. (2009) studied the effect of turbulence models and convection schemes on CFDShip-Iowa V4 (Carrica et al., 2007) resistance prediction using a 1.27M grid. The anisotropic Reynolds stress (ARS) model showed significant improvement over the blended  $k-\omega/k-\varepsilon$  (BKW) model. However the total variation diminishing (TVD) convective scheme did not show significant improvement over the upwind scheme.

Even though the flow pattern for this case is well studied, the vortical structures and their interaction with the hull boundary layer are not yet completely understood. The sparse experimental data documents the flow pattern at several axial cross planes, but is not sufficient to identify the evolution of the vortical structures. Herein, a large grid V4-DES simulation using BKW is performed to evaluate the capability of DES in predicting integral variables, vortical structures and resolved turbulence. A coarse grid URANS using ARS and wall-function (WF) models are also presented for comparison purposes.

The near-wall resolution using immersed boundary method (IBM) is prohibitively expensive for high  $Re$  ship flows. A WF wall-layer model helps in alleviating the grid resolution requirements, but requires large grids compared to curvilinear grid solvers to achieve the ideal near-wall distance  $y^+ = 30$ . Herein, simulations are performed using CFDShip-Iowa V6 (Yang et al., 2008; Yang and Stern, 2009) to evaluate the WF wall-layer modeling with the immersed boundary method.

## 3. NUMERICAL METHODS

CFDShip-Iowa toolbox includes curvilinear (V4) and Cartesian (V6) grid solvers. V4 is currently the work-horse code for ship resistance, propulsion, seakeeping and maneuvering simulations. V6 is a research code which is being turned into a ship hydrodynamics code, and has been previously applied to several fundamental problems such as wave breaking, bubble entrainment and air layer drag reduction. The modeling, numerical methods and HPC of both solvers are discussed below. Readers are referred to Bhushan et al. (2010) for a complete list of the references.

### 3.1 CFDShip-Iowa V4

Modeling: The general-purpose code V4 solves the URANS/DES equations in the liquid phase of a

free-surface flow. The governing equations are solved in absolute inertial earth-fixed or relative inertial coordinates for an arbitrary non-deforming control volume. The turbulence modeling is performed using BKW or ARS models and has DES and WF options. The interface modeling is performed using level-set methods. A multi-block dynamic overset grid approach is used to allow relative motions between the grids for 6DoF ship motions. The overset grid interpolation is performed using SUGGAR. The code provides propeller modeling using simplified body-force or direct discretization, and has a proportional-integral-differential controller to allow self-propulsion or auto-piloted simulations. A semi-coupled two phase flow version of the code with thermal and solute transport capability is also available, where the air flow is solved using the water velocity as boundary condition. (Huang et al., 2008).

**Numerical Methods:** The governing equations are discretized using node-centered finite difference schemes on body-fitted curvilinear grids and solved using a predictor-corrector method. The time marching is done using a second-order backward difference scheme, the convection terms are discretized using a hybrid second/fourth-order linear scheme, and a hybrid first/second-order TVD scheme is used for the level-set equation. First and second-order schemes are also available, but are not used in this study. The equations are solved using implicit schemes. The pressure Poisson equation is solved using the PETSc toolkit and projection algorithms are used to satisfy continuity.

**High Performance Computing:** MPI-based domain decomposition is used for parallelization, wherein each grid block is partitioned into sub-blocks by the user by specifying the number of times the grid needs to be split in the I, J and K directions. Then each sub-block is mapped to a processor. An exact load balance cannot be achieved for a general application, as the number of grid points in a direction may not be divisible by the number of splits or due to the differences in the grid block size. However, the load balance is achieved within 5% on each processor. Recently, Carrica et al. (2010) performed an extensive profiling using the PETSc user-defined events to identify bottlenecks of the in-processor and inter-processor procedures. The HPC performance was improved by optimizing the serial and parallel execution of routines and overset grid assembly resulting in up to 10 times speedup for large grids. The memory usage was improved to avoid the use of shared memory for better scalability on distributed memory machines. For this purpose a scalable partial differential equation-based reinitialization was added as an alternative to the geometrical reinitialization. The most important improvements for the overset assembly included, implementation of SUGGAR as a library to be executed on a dedicated MPI rank and limiting the grid search by using preassembly for motions. The solver shows good scalability up to 2048 processors where the speedup drops 37% below the ideal scaling (Bhushan et al., 2010). The scalability bottlenecks are

identified to be the pressure Poisson solver which requires 72% of the CPU time and SUGGAR interpolation for motions. Based on the scalability studies it was estimated that the largest simulation using V4 on current 2Gb/core HPC systems can be performed using 490M grid points with 2048 processors. The ability to use even larger grids is expected as machines with better memory and cache become available and the code memory usage is further optimized.

### 3.2 CFDSHIP-IOWA V.6

**Modeling:** The URANS/DES/LES equations for two-phase turbulent flows are solved in absolute inertial earth-fixed coordinates using IBM on Cartesian grids. Turbulence is modeled using either BKW or  $k-g/k-\epsilon$  (BKG) models with WF for URANS or a dynamic Smagorinsky SGS model for LES. The WF model include a multi-layer model implemented using a two-point approach (Bhushan et al., 2009). The WF provides the boundary conditions at the immersed boundary using the velocities at a selected probe point. The probe point is selected in the fluid phase along the wall normal direction located at least twice the wall distance of the immersed boundary point or one cell size. The interface is modeled using level-set, particle level-set or coupled level-set and volume-of-fluid (Wang et al., 2009) methods. The level-set model is used in this study

**Numerical Methods:** The governing equations are discretized using finite differences on a non-uniform staggered Cartesian grid and solved using a four-step fractional-step method. Time marching is performed with a second-order Adams-Bashforth scheme; the convection term is discretized using the QUICK or high-order (third or fifth) WENO schemes. The fifth-order schemes are used in this study. The level set evolution and reinitialization equations are solved using the third-order TVD Runge-Kutta and fifth-order HJ-WENO schemes. A semi-implicit scheme can be used for the time marching, but the explicit schemes are used here. The pressure Poisson equation is solved using the Krylov subspace based multi-grid solver in PETSc or the semi-coarsening multi-grid solver in the HYPRE library, and the latter is used herein.

Recently, the immersed boundary approximate domain method (ADM) (Kang et al., 2009) was incorporated to improve the pressure solution near the immersed boundary. For this purpose the ADM boundary was located one cell away from the body as shown in Fig. 1, the cells intersected by the body were removed from the pressure Poisson solver and zero net flux was enforced through the boundary. The implementation of ADM is expected to improve WF predictions as the coupled fluid-solid pressure field with a velocity jump from WF at the immersed boundary causes unphysical large flux near the boundary.

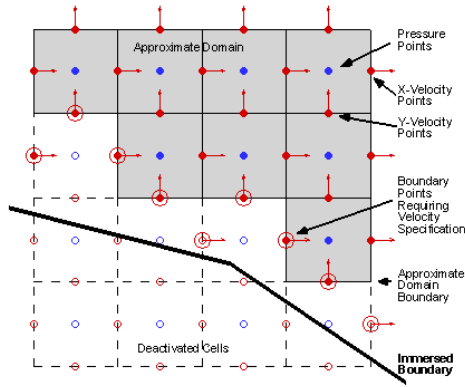


Fig. 1 Illustration of the grid, body, active and deactivated cells for the approximate domain immersed boundary pressure solver.

**High Performance Computing:** The code uses MPI-based domain decomposition and MPI-I/O for solution on HPC platforms. Recent HPC developments were performed by Yang et al. (2008), where the one-dimensional slab decomposition was extended to three directions for parallelization. The solver allows only even splitting of the grids such that an exact load balance can be achieved on each processor. However, the load balance is affected by the uneven distribution of the air-water interface and IBM overhead. The inter-processor communications for the ghost cell information exchange were changed into non-blocking mode. A parallel I/O using MPI2 was implemented such that all the processors read from and write to a single file simultaneously. The solver shows good scalability up to 2048 processors where the speedup drops 25% below the ideal scaling (Bhushan et al., 2010). The scalability bottleneck is identified to be the pressure Poisson solver, which requires 91% of the CPU time. The scalability studies suggest that the largest grid that can be used on current HPC systems is about 1 Billion points. The code has not yet undergone an extensive optimization process similar to V4, thus further improvements are expected. Overall, V6 has advantages over V4 for numerical accuracy and scalability, requires 50% less memory and 20-25% less CPU time per time step per grid point than V4, which makes it better suited for large grid computations.

### 3.3 Domain, Grids, Boundary and Simulation Conditions

The simulations are performed for half hull only as shown in Fig. 2. The domain sizes are  $X/L_{PP} = [-1, 3]$ ,  $Y/L_{PP} = [0, 3]$  and  $Z/L_{PP} = [0.25, -1]$  in the streamwise, spanwise and normal directions, respectively. The V4-DES simulation is performed using a 300M grid on 1461 processors with time step size of  $5 \times 10^{-4}$  for 4 flow times. This required about 110 hours of clock time and a total of 160K CPU hours. The V4-ARS and -WF simulations are performed on a 615K grid on 8 processors with time step size of  $2 \times 10^{-3}$  for 4 flow times. This required 16 hours of clock time and a total of 128 CPU hours. V6-WF simulations are performed on three grids consisting of 34M points with  $y^+ = 150$ , 92M points with  $y^+ = 60$  and 276M points with  $y^+ = 30$ . The 276M grid simulation is

performed using 384 processors with a time step size of  $1.75 \times 10^{-5}$  with periodic time striding, i.e., time step size is increased to  $8.75 \times 10^{-5}$  every  $10^{\text{th}}$  time step. The simulation is performed for 1.53 flow times, which required about 900 hours of clock time and a total of 350K CPU hours. The V6-WF with ADM simulation is performed using the 276M grid restarting from the V6-WF simulation. The simulation is performed for 1 flow time.

A uniform inlet and convective exit boundary conditions are applied at the X-Min and X-Max planes, respectively. A symmetry boundary condition is applied at  $Y/L_{PP} = 0$  and far-field conditions at rest of the boundaries. The near-wall simulations use no-slip boundary conditions at the wall, i.e.,  $J=1$ . In the WF simulations a multi-layer model used to specify velocities and turbulence quantities at  $J=2$  plane or at immersed boundary points in V4 and V6, respectively. The simulations are performed for Case 3.1b conditions, i.e.,  $Re = 5.13 \times 10^6$ ,  $Fr = 0.28$ , sinkage =  $1.92 \times 10^{-3}$  and trim =  $0.136^\circ$ .

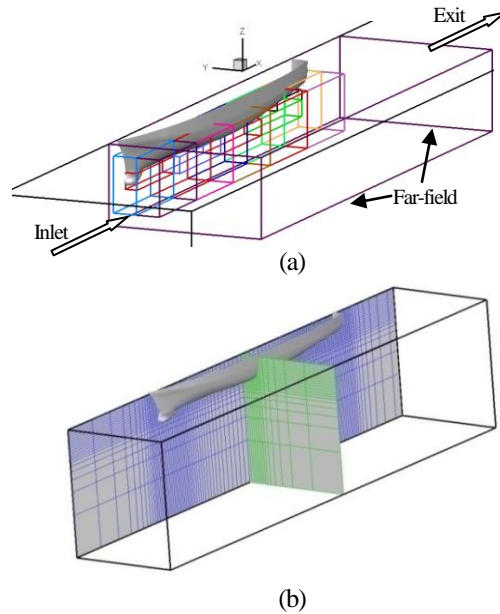


Fig. 2 The domains for (a) V4-DES and (b) V6-WF simulations.

## 4. FIXED SINKAGE AND TRIM 5415

### 4.1 CFDShip-Iowa V4

The grid verification study is not performed, thus the validation study includes only the comparison errors. The resistance predictions show  $E = 2.6\%D$ ,  $7.8\%D$  and  $4.2\%D$  for V4-DES, V4-ARS and V4-WF, respectively. V4-DES predictions are better than those reported by Wilson and Stern (2002), whereas the poor V4-ARS predictions are likely due to coarse grid resolution.

The measured wave elevation displays the so-called Kelvin wave pattern consisting of diverging and transverse waves within a half envelope angle  $\alpha = 19^\circ$ . Both V4-DES and -URANS predict the Kelvin wave half envelop angle well,

however in URANS the waves are diffused and dissipated away from the hull. V4-DES predicts the peaks and troughs in the wave-cuts well. The peaks compare well with the Olivieri et al. (2001) data, but are over predicted compared to Longo et al. (2007) data. V4-URANS predicts lower peaks than the experiments and fails to predict the peaks and troughs for the farthest wave-cut location. Overall, averaged  $E = 3\%D$  and  $8\%D$  for V4-DES and -URANS predictions, respectively.

The vortical structures predicted by V4-DES are shown in Fig. 3a using iso-surfaces of normalized helicity  $Q = 100$  on the starboard side. Symmetric vortices with opposite axial vorticity are predicted on the port side. The results show dominant sonar dome and fore-body keel vortices and relatively weak after-body keel, after-body counter rotating and transom vortices. The sonar dome vortex initiates on the side of the sonar dome surface and evolves in the wake below the hull boundary layer aligned with the center-plane. The fore-body keel vortex initiates at the intersection of sonar dome trailing edge and the keel, and interacts with the hull boundary layer causing a bulge in the boundary layer profile. The sonar dome vortex lifts toward the hull and both the sonar dome and fore-body keel vortices drift away from the center-plane around mid-girth  $x/L = 0.6$ . The sonar dome vortex wraps around the fore-body keel vortex at  $x/L = 0.8$ , which generates the after-body counter-rotating vortex. The merged sonar dome/fore-body keel and the after-body counter-rotating vortices interact with the hull boundary layer causing a bulge in the boundary layer profile at the nominal wake plane. The after-body keel vortex is formed from the keel at  $x/L = 0.8$  and evolves aligned with the hull. The transom vortices are predicted aft of the partially wetted transom stern. As shown in Fig. 3b, V4-ARS predicts the inception of sonar dome and fore-body keel vortices well, but they dissipate quickly downstream and the vortical structures are not captured after  $x/L = 0.4$ . V4-WF predictions are similar to those of V4-ARS, but shows slightly higher diffusion and dissipation.

The sparse experimental data axial vorticity contours and cross flow streamlines at selected axial cross planes in Fig. 4 show a dominant sonar dome and poorly resolved fore-body keel vortices at  $x/L = 0.2$ , sonar dome and fore-body keel vortices at mid girth, and a diffused merged sonar dome/fore-body keel vortex and poorly resolved weak after-body keel and after-body counter-rotating vortices at the nominal wake plane. V4-DES provides a plausible description of the vortical structures observed in the experiment. However, the vortex strengths are higher due to lower dissipation as the turbulence is not resolved, which is discussed later. Both V4-ARS and -WF fail to predict the closed streamlines at the mid-girth and the vortex strengths are significantly weak due to excessive diffusion and dissipation.

Longo et al. (2007) identified that the mean axial and turbulent flow pattern at the nominal wake plane are similar to the boundary layer and turbulence structure in the presence of common-down axial vortex pair. V4-DES helps

identify the vortex pair to be the starboard and port side merged sonar dome/fore-body keel vortices. The vortex pair transports high momentum fluid towards the center plane thinning the boundary layer, whereas the low momentum fluid is transported away from the hull causing a bulge in the boundary layer. V4-DES over predicts the boundary layer bulge due to the over prediction of vortex strength. Both V4-ARS and -WF perform relatively well with slightly thicker boundary layer and under predicted bulge even though the vortices are excessively diffused and dissipated.

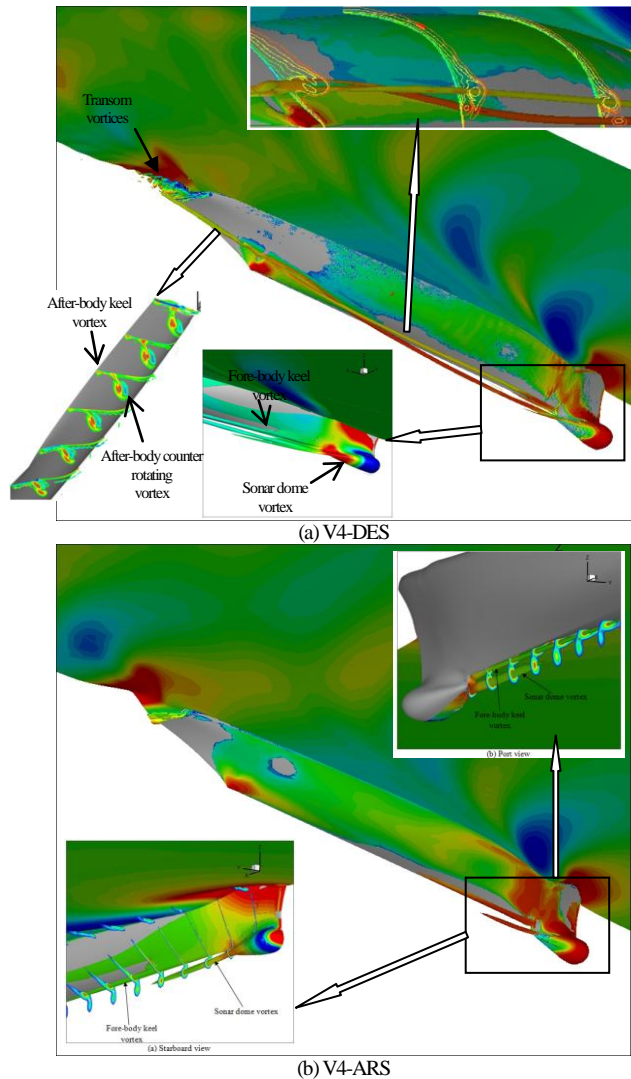


Fig.3 Iso-surface of normalized helicity  $Q = 100$  obtained using (a) V4-DES and (b) V4-ARS.

V4-DES does not predict the turbulence structures well, as the turbulent fluctuations are not activated, i.e., resolved TKE is 25% of the total TKE. The absence of turbulent fluctuations (or turbulent eddy viscosity) explains the lower vortex dissipation. V4-ARS TKE and stress predictions compare qualitatively well with the experiments, however only the TKE, axial normal and  $uv$  shear stresses are predicted quantitatively well. The normal stresses in the other directions and  $uw$  shear stresses are over predicted by

as much as  $60\%D$ . V4-WF shows a penalty in the turbulence prediction both qualitatively and quantitatively.

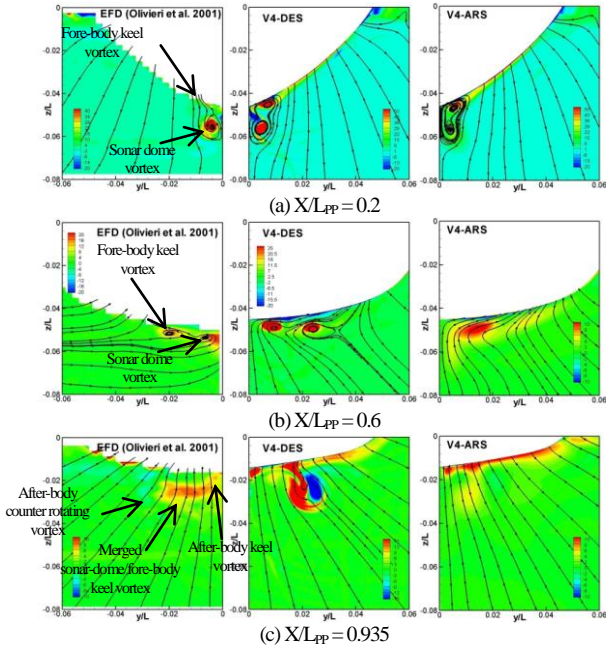


Fig.4 Contour of axial vorticity and cross flow streamlines obtained using V4-DES and V4-ARS are compared with experimental data.

#### 4.2 CFDSHIP-IOWA V.6

In V6, the resistance calculations are not yet possible, thus resistance coefficients are not validated. The Kelvin wave predictions are in good agreement with the experiments for all the grids. However, the transom wave predictions improve with the decrease in  $y^+$ . V6-WF with ADM does not show significant influence on the wave elevation predictions. V6-WF with  $y^+ = 30$  wave-cut predictions show slightly better agreement with Olivieri et al. (2001) data than V4-DES. The averaged  $E = 3\%D$  for the entire wave elevation is comparable to those obtained for V4-DES.

V6-WF with  $y^+ = 150$  fails to predict the fore-body keel vortex and predicts a significantly diffused sonar dome vortex. The fore-body keel and sonar dome vortex predictions improve with the decrease in  $y^+$ . As shown in Figs. 5a and 6a, V6-WF with  $y^+ = 30$  predicts all the vortical structures observed in V4-DES. However the fore-body keel vortex merges with the sonar dome vortex even before the mid-girth. The after-body keel vortex strength is higher than V4-DES, and merges with the merged sonar dome/fore-body keel vortex. Overall, V6-WF predicts diffused vortical structures and the merged sonar dome/fore-body keel vortex is closer to the center-plane compared to V4-DES. V6-WF with ADM in Fig. 5b shows a massive separation from the sonar dome surface, which drifts away from the hull. Thus a well defined sonar dome vortex is not predicted at  $X/L_{pp} = 0.2$  in Fig. 6b. A fore-body keel vortex is observed close to the hull aligned with the center plane both at the inception and mid girth. The poor predictions of the vortical structures and their evolution are

probably due to the poor prediction of the sonar dome vortex. The sonar dome vortical structure resembles vortices shed by a blunt body at low  $Re$ , which suggests that the ADM boundary is located quite far from the body, thus the geometry is not properly resolved.

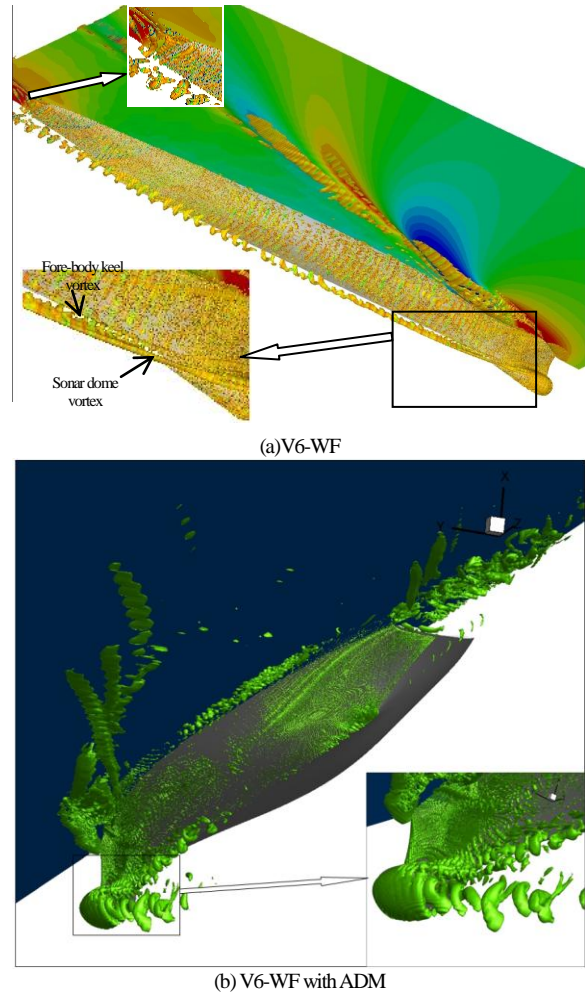


Fig.5 Isosurface of normalized helicity  $Q = 100$  obtained using (a) V6-WF and (b) V6-WF with ADM using 276M grid.

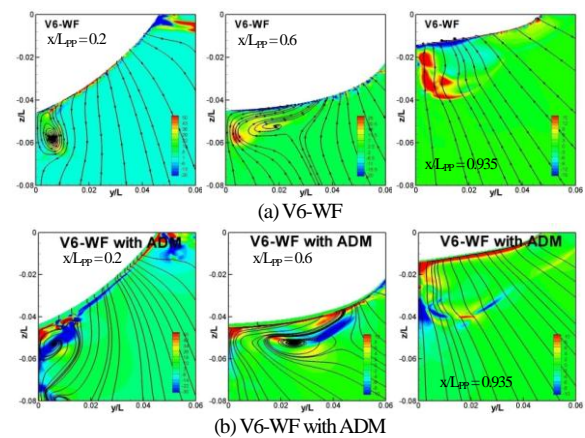


Fig.6 Contour of axial vorticity and cross flow streamlines obtained using V6-WF and V6-WF with ADM using 276M grid.

V6-WF boundary layer predictions improve with the decrease in  $y^+$ , but even with  $y^+ = 30$  the boundary layer bulge is over predicted and is closer to the center-plane compared to the experiments. The latter predicts TKE and stress profiles similar to the experiments, but the peak TKE and the shear stress minima are closer to the center-plane and their magnitudes are over predicted by 40-60% $D$ .

## 5. CONCLUSION

The large grid V4-DES and the coarse grid URANS resistance predictions compare within 2.6% $D$  and 6% $D$  of the experimental data, respectively. V4-DES also shows significant improvements in the wave elevation predictions over URANS, where the comparison errors are 3% $D$  and 8% $D$ , respectively. V4-DES provides a plausible description of the vortical structures and mean flow patterns observed in the sparse experimental data, and helps identify the common-down axial vortex pair at the nominal wake plane to be the port and starboard merged sonar dome/fore-body keel vortices. However, the vortex strengths are over predicted compared to the experiment as the turbulence is not resolved. Further investigation using finer grids are required to understand the resolved turbulence issue, which may lead to the need for advanced turbulence models such as the delayed DES or synthetic turbulence forcing at the inlet or the interface of URANS and LES. The coarse grid URANS performs quite well in predicting the boundary layer and turbulence structures at nominal wake plane, but fails to capture the evolution of vortical structures. Further simulations need to be performed on finer grids to obtain benchmark URANS results. Experiments with even higher resolution are required to capture the inception of the fore-body keel vortex and the vortical structures at the nominal wake plane.

V6-WF wave elevation predictions are within 3% $D$  of the experiment and perform slightly better than V4-DES for the wave-cuts. The vortical structure and boundary layer predictions for 5415 in the straight ahead condition improve with the decrease in  $y^+$  due to the reduction in modeling error. However, even with the ideal WF resolution of  $y^+ = 30$  the vortical structures are diffused, the boundary layer bulge is over predicted and the turbulence quantities are over predicted by 40-60% $D$  compared to the experiments. V4 results show that the WF have some limitations in predicting turbulence quantities, but does not explain the significantly higher turbulence predictions in V6-WF. However, the poor fore-body keel vortex prediction suggests that the wall-layer is not properly resolved probably due to the limitations of WF implementation with immersed boundaries. An approximate domain pressure solver is implemented to decouple the pressure solutions across the immersed boundary to improve the WF predictions. Some preliminary results using ADM suggests that the approximate domain boundary is not specified properly, which results in loss of geometry information. Further study using simple geometries, such as Wigley hull, is required to validate approximate domain method

implementation. Future work will also focus on the implementation of force calculations which may provide additional insight in the boundary layer predictions.

## ACKNOWLEDGEMENT

This research is sponsored by the Office of Naval Research under grants N00014-01-1-0073 and N00014-06-1-0420, administered by Dr. Patrick Purtell. The computations were performed at DoD Navy HPC systems Einstein (XT5) and DaVinci (IBM P6).

## REFERENCES

- Bhushan, S., Xing, T., Carica, P.M., and Stern, F. (2009), "Model- and full-scale URANS simulations of Athena resistance, powering and seakeeping, and 5415 maneuvering," *Journal of Ship Research*, 53(4):179-198.
- Bhushan, S., Carica, P., Yang, J. and Stern, F. (2010), "Scalability studies and large grid computations for surface combatant using CFDSHIP-IOWA," submitted to *The International Journal of High Performance Computing Applications*
- Carica, P. M., Wilson, R. V., and Stern, F. (2007), "An Unsteady Single-phase Level Set Method for Viscous Free Surface Flows," *International Journal of Numerical Methods in Fluids*. 53(2): 229-256.
- Carica, P. M., Huang, J., Noack, R., Kaushik, D., Smith, B., and Stern, F. (2010), "Large-scale DES computations of the forward speed diffraction and pitch and heave problems for a surface combatant," *Computers and Fluids*. 39(7), 1095-1111.
- Hino, T. (2005), Proceedings of the CFD Workshop Tokyo 2005, National Maritime Research Institute, Tokyo, Japan.
- Huang, J., Carica, P. M., and Stern, F. (2008), "Semi-coupled air/water immersed boundary approach for curvilinear dynamic overset grids with application to ship hydrodynamics," *International Journal Numerical Methods Fluids*. 58: 591-624.
- Seongwon Kang, S., Iaccarino, G., Ham, F. and Moin, P. (2009), "Prediction of wall-pressure fluctuation in turbulent flows with an immersed boundary method," *Journal of Computational Physics*, 228, 6753-6772.
- Larsson, L., Stern, F. and Bertram, V. (2000), Proceedings of Gothenburg 2000- A workshop on numerical ship hydrodynamics, Chalmers University of Technology, Gothenburg, Sweden.
- Sakamoto, N., (2009), "URANS and DES simulations of static and dynamic maneuvering for surface combatant," *Ph.D. Thesis*, The University of Iowa.
- Wilson, R. and Stern, F. (2002), "Verification and Validation for RANS Simulation of a Naval Surface Combatant," *AIAA 2002-0904 Aerospace Sciences Meeting*, Reno, Nevada.
- Wang, Z., Yang, J., Koo, B., and Stern, F. (2009). "A coupled level set and volume-of-fluid method for sharp interface simulation of plunging breaking waves," *International Journal of Multiphase Flow*. 35 (3): 227-246.
- Yang, J., Bhushan, S., Suh, J. S., Wang, Z., Koo, B., Sakamoto, N., Xing, T. and Stern, F. (2008), "Large-eddy simulation of ship flows with wall-layer models on Cartesian grids," 27<sup>th</sup> Symposium on Naval Hydrodynamics, October 5-10, Seoul, Korea.
- Yang, J. and Stern, F. (2009), "Sharp interface immersed-boundary/level-set methods for wave-body interactions," *Journal of Computational Physics*. 228(17):6590-6616.